

The Effect of Oil Extraction on Porosity and Methane Adsorption for Dry and Moisture-Equilibrated Shales

Equilibrated Shales

Wei Li¹, Lee A. Stevens*¹, Will Meredith¹, Clement N. Uguna¹, Christopher H. Vane², Bo Zhang³, Andrew D. Carr⁴, Dingye Zheng⁵, Colin E. Snape¹

1. University of Nottingham, Low Carbon Energy and Resources Technologies Group, Faculty of Engineering, Energy Technologies Building, Triumph Road, Nottingham NG7 2TU, UK.

2. British Geological Survey, Centre for Environmental Geochemistry, Keyworth, Nottingham NG12 5GG, UK.

3. Schlumberger Technologies (Beijing) Ltd, Beijing 100000, China.

4. Advanced Geochemical Systems Ltd., 1 Towles Fields, Burton-on-the-Wolds, Leicestershire LE12 5TD, UK.

5. State Key Laboratory of Petroleum Resources and Prospecting, China University of Petroleum (Beijing), Beijing, 102249, China.

* Corresponding author, Lee.Stevens@nottingham.ac.uk

Abstract

The porosity and methane adsorption capacity of shale used to estimate gas in place (GIP) are affected both by moisture and oil residing in the pore structure. As well as oil naturally present from maturation, this can include contaminant drilling mud fluids used for drilling. To demonstrate the impact of extractable oil on methane adsorption capacity for both dry and moisture-equilibrated shales, two overmature shales from China (SH1, SH2) and two lower mature shales from UK (BS3, GH4) have been investigated. The oils extracted in low yield from the overmature shales (<0.5 wt.% TOC) arise from oil-based drilling mud, while the much higher yields from the lower maturity UK shales (1.1-2.5 wt.% TOC) is mainly oil generated by maturation. After extraction, minimal changes

24 (<5%) in total nanopore volume (<100 nm) were observed for the dry over mature shales, but
25 significant increases (95 and 176%) were observed for the dry lower maturity shales. More than 60%
26 of the extracted oil resides in micro and mesopores, and removal could unblock the micropore necks
27 and enlarge the accessible meso and macropore volume. Moisture contents are lower for extracted
28 shales, with reductions of 7-37% observed. Methane equilibrium adsorption capacities increased
29 after oil extraction for both the dry and wet shales, especially for lower maturity shales, where
30 increases were over 200% for the wet shales. Henry's Law was used to show that there were not
31 significant amounts of dissolved methane in oils for the dry shales. Extracting oil from shales prior
32 to determining the porosity and methane adsorption capacity can lead to the GIP being over-
33 estimated for moisture equilibrated shales, particularly for oil-window shales where a reduction of
34 22% was obtained for the shale investigated here.

35 **Key words:** Shale; Maturity; Oil extraction; Methane adsorption; Gas in place.

36 **Highlights:**

- 37 1. Over 60% extractable oil from oil-window shale is stored in the micro-mesopores.
- 38 2. Oil extraction has limited impacts on overmature dry shales.
- 39 3. Moisture contents of wet shales reduce by 7-37% after oil extraction.
- 40 4. Extraction increases micropore and methane adsorption capacities up to 282%.
- 41 5. GIP for oil-window shale can be over-estimated up to 22% by extracting the oil.

42 1. Introduction

43 The organic matter in shales comprises mainly the insoluble organic matter, kerogen (typically >
44 90%), with small amounts of extractable bitumen or oil (typically <10%) [1] removed with common
45 organic solvents [2-4]. Thermal maturity is the critical parameter to indicate the evolution stages of
46 shale oil and gas generation [5, 6]. Shale can be categorized as thermally immature, mature, high
47 maturity, and post or over-mature in terms of capability to generate hydrocarbons. Immature shales
48 with vitrinite reflectance (VR) less than 0.5% Ro, may generate biogenic natural gas. Shales with VRs
49 ranging from 0.5 to 1.3% Ro are in the 'oil window'. High mature shales, VR within the range 1.3-2%
50 Ro in the 'gas window' will generate mainly relatively wet gas, while overmature shales (VR>2% Ro)
51 will generate only dry gas [5-7]. Free gas is stored in the available pore volume, adsorbed gas is
52 mainly in micropores with the greatest surface area, and some gas can dissolve in any hydrocarbons
53 and/or water present [8-12]. Pore networks in shale control the storage and migration of
54 hydrocarbons [13, 14]. The accurate determination of adsorbed gas capacity and porosity is
55 essential for estimating the shale gas in place (GIP), where dissolved gas is normally considered
56 being a relatively minor factor [8, 10, 11, 13, 15].

57 Both initial [9, 16-18] and solvent extracted [14, 19] shales have been used to relate key factors,
58 including temperature, pressure, composition, and moisture impact on the methane adsorption
59 capacity. The difference between initial and extracted dry shales on porosity and methane
60 adsorption capacity has been studied recently [4, 20-24]. Solvent extraction increases specific
61 surface area (SA) [21, 25]. Methane adsorption in shales can potentially be affected by methane
62 dissolving in any oil present [20-24]. Apart from natural oil arising from maturation [3, 23], oil-based
63 drilling muds, in particular, can also impact methane adsorption and gas dissolution [26]. Oil-based
64 drilling muds are widely used as they do not hydrate active clay minerals, and they can affect further
65 analysis unless proper cleaning methods are applied [2, 27]. Previous researchers have reported

66 that the methane adsorption capacities of the dry extracted shales are larger than for the initial
67 shales [20, 21, 23, 25]. As an example, shales were wiped with dry cloths to remove any drilling fluids
68 before extraction [28]. Different extracted solvents (acetone, tetrahydrofuran (THF), carbon
69 disulfide (CS₂), and benzene) have different impacts on extraction yields since they have different
70 molecular dynamics diameter, aromaticity, boiling point, and polarity, which can lead to various
71 effects on porosity and methane adsorption. However, all these studies on the impact of solvent
72 extraction on methane adsorption and pore characteristics of shales were carried out on dry shales.
73 Water exists under reservoir conditions and moisture significantly reduces the methane adsorption
74 for coals and shales [29-32], making researchers focus on moisture equilibrated shales [10, 14, 33-
75 37]. Water reduces gas adsorption by occupying pore volume and blocking the pore necks, and the
76 GIP estimated for moisture-equilibrated shale is considered more accurate [14, 15]. Gas adsorption
77 for wet shales before and after solvent extraction could be different due to the combined influence
78 of moisture and oil on the pore network. However, to date, the combined impact of moisture and
79 residual oil on the porosity and methane adsorption capacities of shales has not been investigated.
80 Furthermore, for dry shales, previous studies have not addressed the influence of extractable oil on
81 GIP estimates.

82 In this study, high-pressure methane adsorption and low-pressure gas sorption were carried out for
83 dry and moisture-equilibrated shale before and after solvent extraction. For the first time, the
84 impacts of solvent extraction on GIP estimations for both dry and moisture-equilibrated shales are
85 revealed. For the shales investigated, the difference between extractable oil that arise from
86 maturation and that introduced as contaminants from oil-based drilling mud is emphasized.

87 2. Experimental Methods

88 2.1 Sample Preparation

89 Two over-mature shales from China were collected from Ordovician-Lower Silurian Wufeng-
90 Longmaxi Formation, south of Sichuan Basin, with the depth of 4119 m for shale 1 (SH1) and 4098
91 m for shale 2 (SH2). SH1 and SH2 were selected from different drilling wells [15]. Two lower mature
92 shales from the UK were collected from the Carboniferous Bowland basin, Beconsall (BS3) from a
93 depth of 2143 m, and Grange Hill (GH4) from a depth of 3113 m. To minimize the effect of sample
94 heterogeneity for the following experiments, all the prepared core shales were crushed and sized
95 to 2-4 mm. For solvent extraction, aliquots of the 2-4 mm particles were further crushed to < 250
96 μm for comparison.

97 The initial and solvent extracted shale samples were both dried and equilibrated at 95% R.H.
98 moisture (wet) for high-pressure and low-pressure gas sorption experiments. The dry shales were
99 prepared in the vacuum oven (<0.5 mbar) at 120 °C for 48 hours before starting any experiments.
100 The wet shales were prepared in a vacuum desiccator containing saturated potassium nitrate (KNO_3)
101 solution (8 g KNO_3 /10 mL H_2O), which can provide $95\pm 2\%$ R.H. moisture equilibration conditions at
102 20 °C [38-40]. A logger was used to monitor the R.H. and the temperature to make sure the shales
103 reach the moisture equilibration after being kept in the desiccator for 48 hours [15]. The moisture
104 contents for the wet samples were calculated from the mass differences.

105 2.2 Soxhlet Extraction

106 Soxhlet solvent extraction was carried out on 20 g of shale using both the 2-4 mm and <250 μm
107 fractions to ensure the particle size has almost no impact on the oil yields. Samples were loaded
108 into the pre-cleaned thimble plugged with cotton by extraction solvent. A mixture of 186 ml
109 dichloromethane (DCM) and 14 ml methanol was used. Extraction was carried out for 120 hours at
110 40 °C. The solvent was removed after extraction using a rotary evaporator at 35 °C under 400 mbar

111 pressure. The remaining solvent (about 2 ml) was then collected into a pre-weighed vial and dried
112 until no weight change. The extracted organics yield was calculated by the mass of oil and TOC.
113 Duplicate extractions for each shale were carried out to collect the remaining solvent (about 2 ml)
114 without drying, which was prepared for the GC-MS analysis.

115 2.3 Elemental Analysis and Vitrinite Reflectance

116 Shales prepared for elemental analysis were ground into powder (<250 μm). 3 g powder initial shale
117 was treated with sufficient hydrochloric acid (HCl), 1 mol/L, to remove the carbonate. The treated
118 samples were washed with distilled water for 6 times until pH 7 is reached. After carefully decanting
119 the water from the samples, samples were dried in the vacuum oven (<0.5 mbar) at 120 °C for 48
120 hrs. Then 120 mg of shale was used to determine the total organic carbon (TOC) using a Leco
121 CHN628 elemental analyzer. 1.5 g particle (2-4 mm) shale was used to prepare the polished blocks
122 for the VR (% Ro), measuring the maturity of shales. For the UK shales, the measurement of
123 recognizable vitrinite was made by a LEICA DM4500P microscope with motorized 4-fold turret for
124 reflectance, and data were collected via the Hilgers Fossil Man system connected to the microscope.
125 For the two Chinese over mature shales, bitumen reflectance (BR) measurements were conducted
126 on the polished blocks because of the lack of vitrinite in the Wufeng-Longmaxi shales. The VR was
127 calculated from the BR according to the equation $VR = (BR + 0.2443)/1.0495$ [41].

128 2.4 Low-pressure gas (N_2 , CO_2) sorption

129 Low-pressure gas sorption experiments were carried out on both initial and extracted dry and wet
130 shales (2-4 mm particles) by a Micromeritics Surface Area and Porosity Analyser (ASAP 2420) to
131 obtain the pore characters of initial and extracted shales. In this study, Brunauer-Emmett-Teller (BET)
132 theory was used to obtain the surface area (SA) from N_2 sorption, where the relative pressure (P/P° ,
133 P is the absolute equilibrium pressure and P° is the saturation pressure) is in the range of 0.05 and
134 0.2 [42, 43]. Non-Local Density Functional Theory (NLDFT) equilibrium model assuming slit pores

135 was used to calculate the pore volume from 0.33 to 100 nm [12, 44, 45]. Compared with the Barrett-
136 Joyner-Halenda (BJH) model, the NLDFT model can give a more realistic description of micropore
137 filling while using the BJH model is always leading to an underestimation of pore sizes of micropores
138 and even smaller mesopores [43, 46-48]. 4 g dry and wet particle shales was used for the low-
139 pressure N₂ sorption experiments, and 2 g dry shale was prepared for CO₂ adsorption.

140 The shale samples were degassed under high vacuum (<0.013 mbar) at 120 °C for 15 hours before
141 dry low-pressure (N₂, CO₂) sorption experiments. To ensure the wet samples were not exposed to
142 vacuum at higher temperatures, the wet shale samples were frozen in liquid N₂ first before manually
143 evacuating the sample tube and starting the low-pressure N₂ sorption analysis. The mass deviation
144 of wet samples before and after analysis was ±0.002%. The P/P° of low-pressure N₂ sorption analysis
145 is set from 10⁻⁷ to 0.995 P/P°, and all the analysis was performed at -196 °C in a liquid N₂ bath. The
146 low-pressure CO₂ sorption analysis was carried out at 0 °C with a P/P° from 6×10⁻⁵ to 3.5×10⁻², with
147 absolute pressure is from 0.002 to 1.2 bar, to characterize the ultra-microporous structure (<0.8 nm)
148 of dry shales [14, 49].

149 CO₂ adsorption was not carried out for wet shales because the experimental temperature is 0 °C
150 which is hard to hold the moisture in the wet sample under low pressure. Besides, there is little or
151 almost no difference between N₂ and CO₂ SA on dry samples, which suggesting N₂ can penetrate all
152 ultra-micropores of wet samples [15]. The free space test by helium on the instrument was not used
153 for the low-pressure gas sorption isotherms since an automatic warm free space test would expose
154 the equilibrated moisture samples to a vacuum which would remove the moisture. Thus, the
155 skeletal densities of wet and dry shales measured by Helium pycnometry were used to calculate the
156 warm and cold free space manually to obtain the correct gas sorption results. The bulk density of
157 dry shales was obtained from Mercury intrusion porosimetry by Micromeritics Autopore IV Series
158 instrument at 0.035 bar [15].

159 2.5 High-pressure methane adsorption

160 High-Pressure Volumetric Analyzer (HPVA-100) was used to measure the high-pressure methane
161 adsorption of shale by the static volumetric method. Approximately 10 g shale particles (2-4 mm)
162 wet and dry were weighed and loaded into the 10 mL stainless steel sample cell and sealed before
163 the measurement. Each sample was analyzed in triplicate to assess errors. For the dry measurement,
164 all the samples in the cell were degassed at 120 °C for 48 hours first, and then the methane
165 adsorption isotherms were acquired. A sample pre-evacuation was carried out for 45 minutes to
166 reach a vacuum setpoint of 0.013 bar on the high-pressure instrument, and an isotherm was
167 generated from 0 to 105 bar with a 45-minute equilibration time per pressure point. For the wet
168 shales, all the methane adsorption isotherms were obtained from 1.2 to 105 bar at 25 °C, avoiding
169 the wet samples being subjected to a vacuum on the high-pressure instrument. The mass deviation
170 of wet shales before and after analysis was $\pm 0.0018\%$. Similar free space corrections were carried
171 out on this instrument as for the low-pressure gas sorption method using skeletal density and
172 manually calculating warm and cold free spaces.

173 The actual adsorbed layer should be represented by the absolute amount, and this is the gas
174 quantity that needs to be considered rather than the surface excess amount obtained by the
175 volumetric sorption measurement. The Gibbs equation (equation (1)) [13, 50] is used in order to do
176 the conversion, since the difference between excess and absolute amount adsorbed is non-
177 negligible at higher pressure exceeding 10 bar [12]. The dual-site Langmuir model, which is suitable
178 for heterogeneous adsorbents [13, 14] is used in this study to predict the methane adsorption at
179 pressures over 105 bar. The equation for the dual-site Langmuir can be written in the following form
180 (equation (2)).

$$181 Q_a = Q_e + (V_a \times \rho_g) \quad (1)$$

182
$$Q_a(P, T) = Q_{max} \times \left[(1 - \alpha) \frac{b_1(T)P}{1 + b_1(T)P} + \alpha \frac{b_2(T)P}{1 + b_2(T)P} \right] \quad (2)$$

183 Where, Q_a is the absolute adsorption quantity; Q_e is the excess adsorption quantity; Q_{max} is the
184 max absolute adsorption quantity; V_a is the pore volume for gas to adsorb into; ρ_g is the density of
185 the bulk gas; $b_1(T)$ and $b_2(T)$ are the temperature-dependent equilibrium constants, which are
186 related to the energy of adsorption sites; $b_1(T)$ and $b_2(T)$ are weighted by a coefficient (α); α is the
187 fraction of the second type of site ($0 < \alpha < 1$); P is the pressure; T is the temperature.

188 2.6 Gas Chromatography-Mass Spectrometry

189 Extracted oils from the shales were analyzed by gas chromatography-mass spectrometry (GC-MS)
190 using Agilent GC-MS (7890B GC; 5977A-mass selective detector (MSD)) in splitless mode. Product
191 separation was performed on an HP-5MS column (30 m × 250 μm × 0.25 μm). The GC oven
192 temperature was initially held at 50 °C for 0.5 min, then heated to 300 °C at a rate of 4 °C/min, where
193 it was held for 5 minutes. The MS (EI of 70 eV) was scanned in the mass range of m/z 40–400, with
194 an ion source temperature of 200 °C. Individual compounds were identified using a NIST 14 MS
195 library and published data.

196 3. Results and Discussion

197 3.1 Shale characterization and geochemistry

198 Basic information on the shales, including their formation, bury depth, TOC, maturity, moisture
199 content of wet samples, and the yield of extracted organic matter, are listed in Table 1. The shales
200 from different formations and depths have TOC contents ranging from 2.4 to 5.1 wt.%. Shales SH1
201 (2.95% Ro) and SH2 (2.58% Ro) are overmature, BS3 (1.01% Ro) is oil-window maturity and GH4
202 (1.95% Ro) is gas-window maturity. The moisture contents of the initial and extracted shales are in
203 the ranges 1.22-2.72 and 1.13-2.06 wt.%, respectively, indicating the extracted shales adsorb less
204 water with reductions of 15, 7, 37, and 25% for SH1, SH2, BS3, and GH4, respectively. The yield of
205 extractable oil decreases with increasing maturity from 2.5 wt.% TOC for the oil-window shale, BS3
206 to 1.1 wt.% TOC for the gas-window shale, GH4, and 0.3-0.5 wt.% TOC for the over-mature shales,

207 SH1 and SH2. The extracted oil volumes range from 0.13 to 0.73 $\mu\text{L/g}$, assuming the extracted oil
 208 density is 0.85 g/m^3 , which is the same as light crude oil [51, 52].

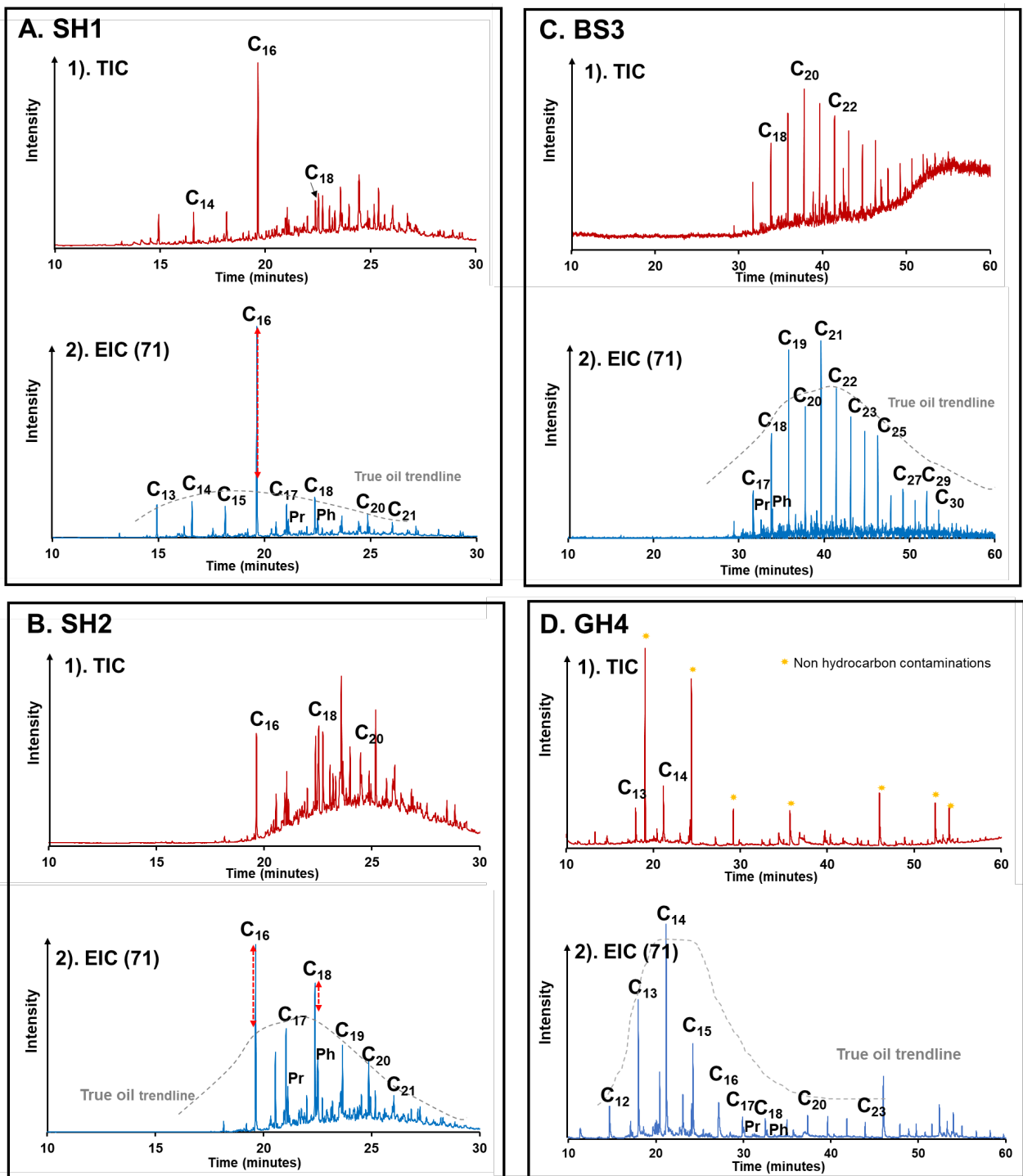
209 Table 1. Characteristics of the initial and extracted shales

Sample	Formation	Depth (m)	TOC (wt.%)	Maturity (% Ro)	Moisture (wt.%)	Oil Yield (wt.% TOC)	Oil volume (V_{oil}) ($\mu\text{L/g}$)
Initial SH1	Ordovician - Lower Silurian Wufeng-Longmaxi, China	4119	5.1	2.95	1.50 ^a	0.3	0.17
Ext SH1					1.27 ^b		
Initial SH2	Ordovician - Lower Silurian Wufeng-Longmaxi, China	4098	2.4	2.58	1.22 ^a	0.5	0.13
Ext SH2					1.13 ^b		
Initial BS3	Carboniferous Bowland Beaconsall, UK	2143	2.5	1.01	1.84 ^a	2.5	0.73
Ext BS3					1.17 ^b		
Initial GH4	Carboniferous Bowland Grange Hill, UK	3113	3.4	1.95	2.72 ^a	1.1	0.44
Ext GH4					2.06 ^b		

210 The TOC, moisture, and oil yield were the average data from triplicate determinations. Moisture^a is the
 211 moisture content for the initial shale, and moisture^b is that for extracted shale.

212 3.2 GC-MS characterization of the extracted oils

213 Figure 1 shows the total ion chromatograms (TIC) and m/z 71 single ion chromatograms (EIC 71) for
 214 the oils extracted from the four shales with the *n*-alkane peaks labelled. The oil from the oil-window
 215 shale, BS3, is characteristic of a paraffinic oil with *n*-alkanes prominent ranging from C_{16} to C_{33} and
 216 the pristane to phytane ratio close to 1 (Figure 1C). Although the Bowland shale is a mixture of Type
 217 II/III and IV kerogens [53, 54], the oil has been generated predominately from the Type II kerogen
 218 present. The yield of oil extracted from the gas-window Bowland shale sample (GH4) was much
 219 lower than that for the oil-window shale (BS3) and is considerably lighter with *n*-alkanes from C_{12} to
 220 C_{23} (Figure 1D). Further, there is evidence of some non-hydrocarbon contamination from siloxane
 221 and methyl esters which are likely to rise from column bleed and the septa of the GC or the vial cap.



223 Figure 1. GC-MS total ion and m/z 71 single ion chromatograms for the extracted oil with the *n*-
 224 alkane peaks labelled. A, B, C, and D are the oils from SH1, SH2, BS3, and GH4.

225 For the two over-mature shales where the extractable oil yields are low, light condensate would be
 226 expected with possibly small quantities of residual oil. The extractable oils are relatively heavy and
 227 contain *n*-alkanes in low concentrations. However, the fact that the *n*-alkanes do not extend beyond
 228 *n*-C₂₃ would suggest that they could arise from a small quantity of remaining oil. *n*-Hexadecane

229 dominant in the extract from SH1 (Figure 1A) is possibly drilling fluid-derived and, similarly, although
230 much less pronounced the slightly elevated concentrations of *n*-hexadecane and *n*-octadecane over
231 the other *n*-alkanes in the extract from SH2 (Figure 1B) [55]. The majority of the TICs for the extracts
232 from the two over-mature shales comprise complex mixtures extending beyond C₃₀. The common
233 drilling mud 'oil' bases including the diesel, enhanced-mineral oil (EMO), and synthetics (olefins and
234 esters). The oil contaminated by the diesel and EMO shows a relatively higher peak of C₁₆ in GC data
235 [55]. The evidence would suggest that EMOs account for most of the complex mixtures extracted
236 from SH1 and SH2.

237 3.3 Impact of solvent extraction impact on nanoporosity

238 The pore SA, micro, meso, macro, total nanopore volumes (pore size less than 100 nm), and their
239 changes after solvent extraction calculated from the low-pressure N₂ and CO₂ gas isotherms are
240 compared in Table 2. The different pore volume percentages for the dry and wet initial and
241 extracted shales are presented in Figure 2. The SA and pore volumes of the dry shales decrease as
242 the maturity decreases, in the order of SH1>SH2>GH4>BS3 (Table 2). This suggests that higher
243 maturity shales generally develop more pores, which is consistent with previous studies [19, 56-59].
244 Although mesopores are dominant in the dry shales (Figure 2), the micropores still occupy a
245 significant fraction of the pore volume. The contributions of micropores to the total nanopore
246 volume are much higher in the over mature shales, SH1 and SH2, than those in the gas-window shale
247 GH4 and oil-window shale BS3 (Figure 2), suggesting hydrocarbon generation facilitates the
248 development of micropores [59-61].

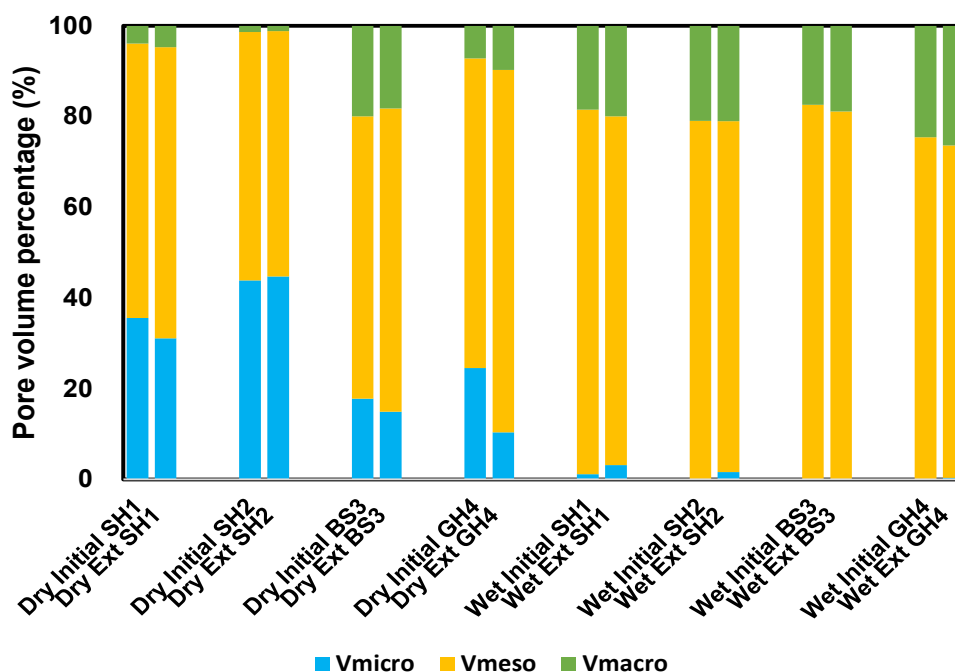
249 Increases in pore volume are expected after any native oil is extracted [3, 28]. However, for the dry
250 over mature shales, the changes (<20 %) in surface area and nanopore volume are small (Table 2)
251 due to the low extraction yields (<0.5wt.% TOC, Table 1), with the extracted material being mainly
252 drilling mud derived. Since the permeability of shales (typically less than 0.001 mD) is very low [62]

253 [63] [64], it is difficult for the drilling muds to penetrate the shale bulk, with most being on the
 254 surface. Solvent extraction may cause additional effects, such as contributing to the swelling of clay
 255 pores by the solvent [65] or changing the interactions with rocks if solvent adsorbing on clay surfaces
 256 or absorbing in kerogens [3, 28], which could interrupt the physical interactions between shales and
 257 adsorbed gas leading the measured SA and pore volume decreasing after extraction.

258 Table 2. Surface area and pore volumes of dry and wet shales.

Sample Name	BET SA(m ² /g)	V _{micro} (μL/g)	V _{meso} (μL/g)	V _{macro} (μL/g)	V _{nano} (μL/g)
Dry Initial SH1	21.73	6.9	11.7	0.75	19.3
Dry Ext SH1	19.11	5.7	11.8	0.87	18.4
SH1 Change*	-12%	-17%	1%	15%	-5%
Dry Initial SH2	16.70	5.37	6.7	0.16	12.2
Dry Ext SH2	16.67	5.42	6.5	0.14	12.1
SH2 Change*	-0.2%	1%	-2%	-17%	-1%
Dry Initial BS3	0.13	0.098	0.34	0.11	0.55
Dry Ext BS3	0.26	0.160	0.72	0.20	1.1
BS3 Change*	92%	64%	110%	78%	95%
BS3 Oil P*	-	9%	52%	12%	73%
Dry Initial GH4	2.19	0.60	1.7	0.17	2.4
Dry Ext GH4	2.62	0.70	5.3	0.7	6.7
GH4 Change*	20%	17%	222%	273%	176%
GH4 Oil p*	-	23%	845%	109%	977%
Wet Initial SH1	0.075	0.0039	0.28	0.063	0.34
Wet Ext SH1	0.059	0.0081	0.20	0.051	0.26
SH1 Change*	-21%	105%	-28%	-19%	-25%
Wet Initial SH2	0.029	0.0	0.21	0.056	0.27
Wet Ext SH2	0.036	0.0033	0.16	0.042	0.20
SH2 Change*	25%	-	-26%	-25%	-25%
Wet Initial BS3	0.060	0.0	0.18	0.038	0.22
Wet Ext BS3	0.108	0.0	0.32	0.07	0.40
BS3 Change*	79%	-	80%	98%	83%
Wet Initial GH4	0.011	0.0	0.07	0.023	0.09
Wet Ext GH4	0.045	0.0012	0.25	0.089	0.34
GH4 Change*	310%	-	257%	295%	268%

259 S_{BET} are the surface areas calculated by BET theory; V_{micro}, V_{meso}, V_{macro}, and V_{nano} are the micropores (<2 nm),
 260 mesopore (2-50 nm), macropore (50-100 nm), and the total nanopore volume (<100 nm) calculated by the
 261 NLDFT model. Change* (in bold) is the change in pore properties resulting from solvent extraction compared
 262 with initial shales. Oil P* is the potential contribution of the increased pore volume to storing the extracted
 263 oil, which is calculated by $Oil\ P^* = 100\% \cdot (V_{Ext\ p} - V_{Ini\ p})/V_{oil}$, where V_{Ext p} is the pore volume of shale
 264 after extraction, V_{Ini p} is the pore volume of initial shale, and V_{oil} is the extracted oil volume (Table 1). Oil P*
 265 was only calculated for BS3 and GH4 since these are the only shales containing oil generated by maturation.



268 Figure 2. Micropore, mesopore, and macropore (<100 nm) volume percentages for the dry and
 269 wet initial and extracted shales.

270 The influence of solvent extraction is much larger for the two lower maturity shales. Table 2
 271 indicates that the SA doubled from 0.13 to 0.26 m²/g for dry BS3 and increased by 20% from 2.19 to
 272 2.62 m²/g for GH4. The total nanopore volume (up to 100 nm) also doubled for dry BS3 (from 0.55
 273 to 1.1 μL/g) and increased by 176% for GH4 (from 2.4 to 6.7 μL/g). If the increased 64% micropore
 274 pore volume is generated solely by removing the oil, it is estimated that 9% of the extracted oil in
 275 shale BS3 is stored in the micropores (Oil p* in Table 2). The mesopores (from 0.34 to 0.72 μL/g) and
 276 macropores up to 100 nm (from 0.11 to 0.20 μL/g) increase by 110 and 78%, respectively, after oil
 277 extraction. This new porosity provides estimated storage space for 52 and 12%, respectively, of the
 278 extracted oil (64% in total). Similarly, for GH4, the increase of 17% micropore volume provides
 279 storage space for 23% oil, with the rest 77% oil stored in the mesopore or/and macropore, since the
 280 mesopores (from 1.7 to 5.3 μL/g) and 50-100 nm macropores volume (from 0.17 to 0.7 μL/g)
 281 increase by over 200% (Table 2). Clearly, for GH4, oil removal opens access to blocked

282 meso/macropores since the increase in pore volume is considerably greater than the volume of the
283 extracted oil. For BS3, where the increase in pore volume accounts for 73% of the extracted oil, the
284 implication is that some of the oil resides in macropores > 100 nm.

285 The aliphatic and aromatic hydrocarbons in oils are mainly stored in micro and mesopores, but the
286 higher molecular mass polars and asphaltenes reside primarily in the macropores [3, 21, 28, 66].

287 The increase in macropore volume for the extracted shale is consistent with the non-hydrocarbons
288 being removed by solvent extraction. The overall nanoporosity increases after extraction for the oil-
289 window shale, BS3, and the gas-window shale, GH4 are larger than SH1 and SH2 since it is oil
290 generated by maturation being extracted, as opposed to drilling fluids residing close to the surface.

291 As expected from our earlier studies [14, 15], most pore volume and SA are lost on wetting the
292 shales (Table 2). Although mesopores are still dominant as for the dry shales, macropores replace
293 micropores as the secondary pores in the wet shales (Figure 2), for both the initial and extracted
294 samples. This arises from most of the micropores or micropore-necks being filled or/and blocked by
295 water [15]. Solvent extraction provides a more complex influence on the pore system of wet shales.

296 For extracted wet over-mature shales, SH1 and SH2, apart from micropore volume increasing (from
297 0.0039 to 0.0081 $\mu\text{L/g}$ for wet SH1, and from 0 to 0.0033 $\mu\text{L/g}$ for wet SH2), the mesopore,
298 macropore and nanopore pore volumes all decrease slightly, with the reduction of -28, -19 and -25%
299 for SH1, and -26, -25, -25% for SH2 (Table 2). The increase of micropores indicates there is less water
300 to fill or block micropores in the extracted shales than initial shales as oil extraction did not enlarge
301 micropores, mesopore, or macropores as discussed above. Larger micropores in extracted wet SH1
302 and SH2 could be due to the solvent interacting and altering the pore surface [3, 23, 28, 67], making
303 it hard for water to condense or block micropores in solvent-extracted shales than initial shales.
304 Additionally, the moisture contents of the extracted shales are also less than those of the initial

305 shales (Table 1), with reductions of 15, 7, 37, and 25% for wet SH1, SH2, BS3, and GH4, respectively,
306 suggesting less water is absorbed.

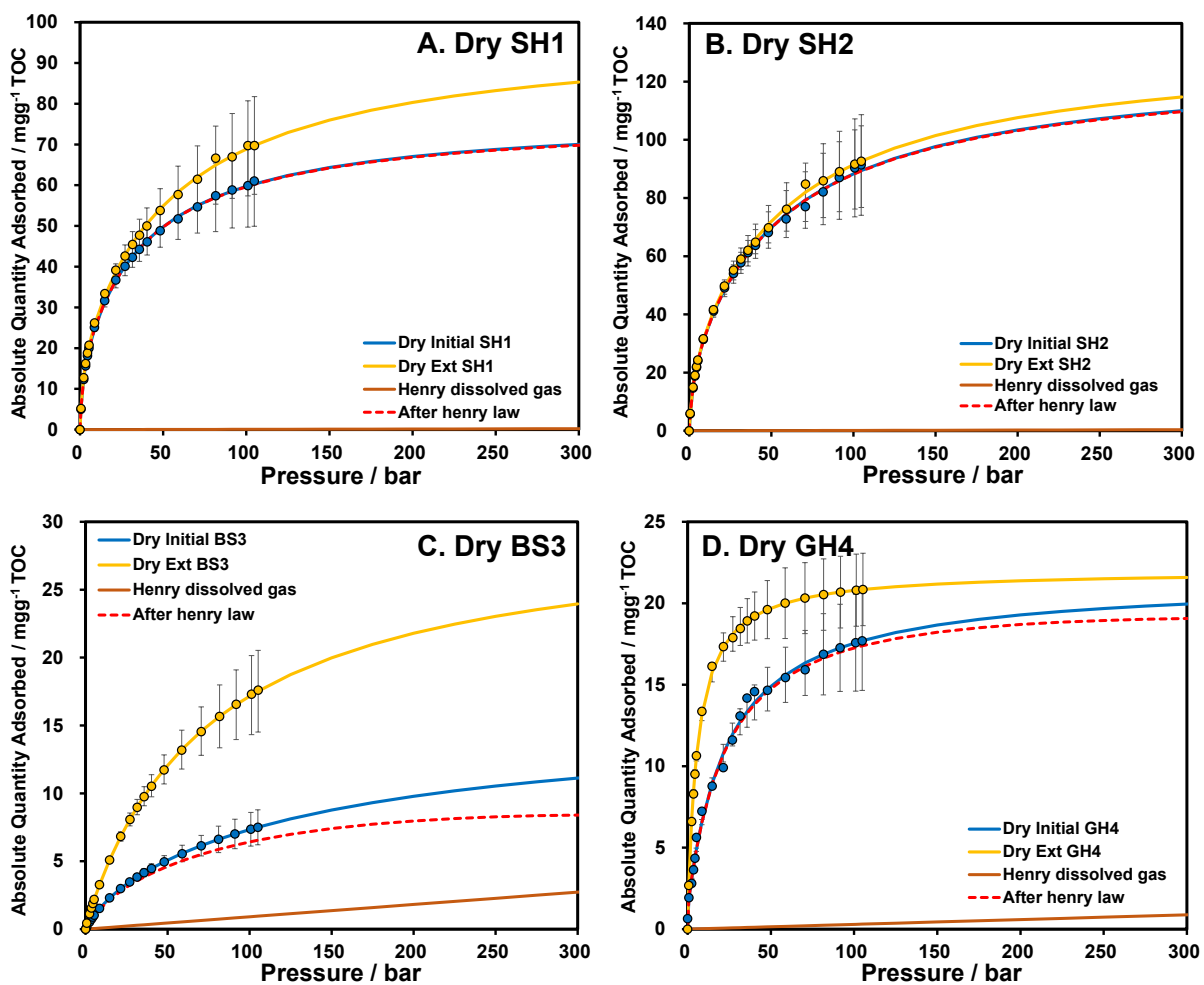
307 For the wet BS3 and GH4 shales, apart from the micropore volume of BS3 remaining close to zero,
308 all the other pore volumes display increases after solvent extraction (Table 2), For BS3, these are
309 80% for mesopores (from 0.18 to 0.32 $\mu\text{L/g}$), 98% for macropores (from 0.038 to 0.07 $\mu\text{L/g}$) and 83%
310 for the total nanopores (from 0.22 to 0.40 $\mu\text{L/g}$) volumes are increasing for wet BS3. Large
311 proportional increases are observed for GH4, the micropores increase from 0 to 0.0012 $\mu\text{L/g}$, being
312 257% for mesopores (from 0.07 to 0.25 $\mu\text{L/g}$), 295% for macropores (from 0.023 to 0.089 $\mu\text{L/g}$) and
313 268% total nanopores (from 0.09 to 0.34 $\mu\text{L/g}$). The increases in wet shales show a similar pattern
314 to dry samples. The pore volume increases for the wet extracted BS3 and GH4 shales are due to a
315 combination of oil removal enlarging the pores and the extracted shales having lower moisture
316 contents.

317 Overall, as well as water, the results indicate that extracted oil can have a significant impact on pore
318 characteristics. Although overmature shales have the largest pore volume, almost no oil remains, as
319 most of the oil has migrated. The limited pore system changes of overmature shales before and
320 after solvent extraction indicate solvent extraction would not destroy the shale original pore system,
321 only changing the interaction of shale pore surface. The oil generated by maturation mainly resides
322 in the pores less than 50 nm (micropores and mesopores) for the early to high mature shales, and
323 removing the oil increases the accessible pore volume no matter for dry or wet shales.

324 [3.4 Impact of solvent extraction impact on methane adsorption](#)

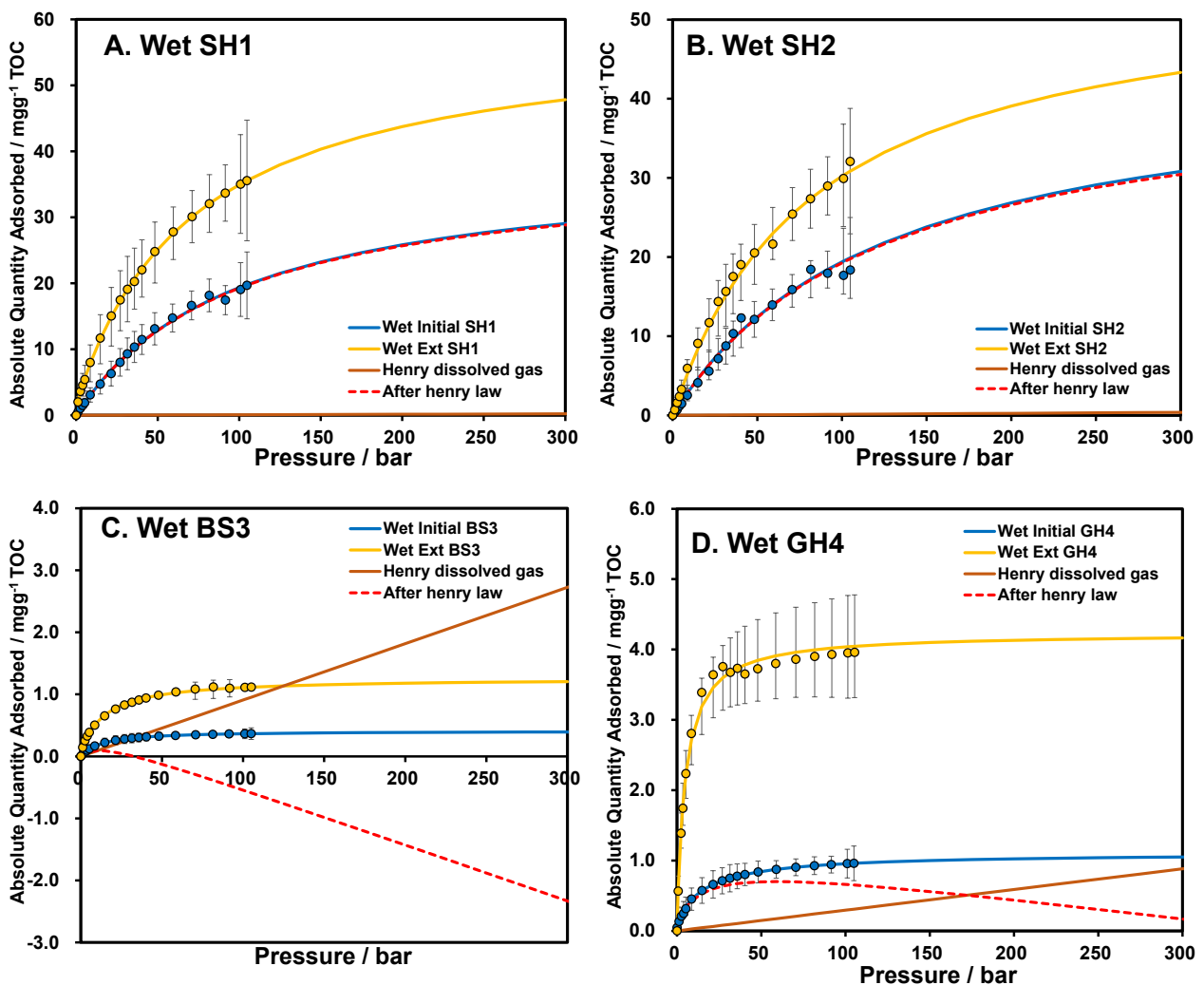
325 The methane adsorption isotherms of the initial and solvent extracted shales are compared in
326 Figures 3 and 4, for the dry and moisture-equilibrated samples, respectively. The equilibrium
327 methane adsorption capacities (Q_m) derived from the isotherms are listed in Table 3. For the initial

328 samples, the solubility of methane in oils has been estimated by Henry's Law, assuming that the
 329 methane is accessible to all the extractable oil. Thus, the estimated amount of adsorbed methane
 330 after Henry's law is the difference between the total amount of methane taken up by the samples
 331 and the dissolved methane estimated by Henry's Law linear plots in Figures 3 and 4. For the dry
 332 samples, the two over-mature shales, SH1 and SH2, have the higher equilibrium adsorption
 333 capacities, 77 and 127 mg/g TOC, respectively, compared to 16 and 21 mg/g TOC, respectively for
 334 the oil and gas window shales, BS3 and GH4, for the dry samples (Figure 3).



336 Figure 3. Methane adsorption isotherms of the dry initial shales, dry solvent extracted shales, after
 337 Henry law correction for initial shales, and the dissolved methane uptakes calculated by Henry's Law.
 338 Shales SH1, SH2, and BS3 have type I(b) isotherms, with shale GH4 having a type I(a) isotherm
 339 displaying a steeper isotherm at low pressures (Figure 3), arising mainly from narrow micropores
 340 (width <1 nm) [43]. For overmature dry shales, SH1 and SH2 (Figures 3A and B), although the average

341 methane adsorption isotherms of extracted shales are higher than the initial shales, with the Q_m
 342 increased 27% (from 77 to 98 mg/g TOC) for SH1 and 5% (from 127 to 133 mg/g TOC) for SH2, they
 343 are still within the error range, suggesting the methane adsorption capacities of initial and extracted
 344 shales are relatively close. Thus, solvent extraction shows little impact on their methane adsorption
 345 capacities. Further, even deducting the potential contribution from dissolved methane in the low
 346 yields of extracted oil, the methane adsorption isotherms after the Henry's Law correction has very
 347 little impact, with the methane adsorption amount at 300 bar ($Q_{300\text{bar}}$ is used as there is no Q_m for
 348 Henry law) changing by only *ca.* 0.3% for SH1 (from 70.0 to 69.8 mg/g TOC) and SH2 (from 110.0 to
 349 109.6 mg/g TOC).



351 Figure 4. Methane adsorption isotherms of the wet initial and extracted shales, showing the Henry's
 352 Law corrections for dissolved methane in the oil present.

353 In contrast to the overmature shales, removing the residual oil increases the methane adsorption
 354 capacities of dry oil-window shale, BS3 significantly (Qm increased 90% from 16 to 30 mg/g TOC), A
 355 smaller increase is observed for dry gas-window shale GH4 (Qm increased 3% from 21 to 22 mg/g
 356 TOC) consistent with the lower yield of extractable oil compared to BS3. A steeper uptake at low
 357 pressure (<50 bar) of extracted GH4 isotherm is observed (Figure 3D), which indicates removing
 358 extracted GH4 oil increases narrow micropores (<1nm) [43], consistent with the oil being relatively
 359 light (section 3.2). Although isotherms are less steep after the Henry's Law correction for dry shales,
 360 the isotherm type remains the same, with their shapes being similar in the low-pressure range (<50
 361 bar, Figure 3). The Henry's Law corrections reduce Q_{300bar} for BS3 (from 11.1 to 8.4 mg/g TOC) (Figure
 362 3C) and GH4 (from 20.0 to 19.1 mg/g TOC) (Figure 3D) by 25 and 4.4%, respectively. However, this
 363 assumes that all the oil is accessible to the methane, if this is not the case, the impact of dissolved
 364 methane will be much less.

365 Table 3. The methane adsorption amount of dry, wet, initial, and extracted shales.

Adsorption (mg/g TOC)	Initial SH1	Ext SH1	<i>Qm</i> Change SH1(%)	Initial SH2	Ext SH2	<i>Qm</i> Change SH2 (%)	Initial BS3	Ext BS3	<i>Qm</i> Change BS3 (%)	Initial GH4	Ext GH4	<i>Qm</i> Change GH4 (%)
Dry Q _{300bar}	70.0	85.3	-	110.0	114.7	-	11.1	24.0	-	20.0	21.6	-
Dry Qm	77	98	27	127	133	5	16	30	90	21	22	3
Wet Q _{300bar}	29.1	47.8	-	30.8	43.3	-	0.4	1.2	-	1.1	4.2	-
Wet Qm	39	59	52	44	55	27	0.4	1.3	207	1.1	4.2	282
Qm Reduction (%)	50	40	-	66	58	-	97	96	-	95	81	-

366 Qm is the equilibrium methane adsorption capacities; Q_{300bar} is the methane adsorption amount at 300 bar;
 367 Q change (%) is the methane adsorption amount changes before and after the extraction; Qm Reduction (%)
 368 is the methane adsorption reduction for wet samples compared with corresponding shales.

369 Methane adsorption capacities of both the initial and extracted shales are reduced after moisture
 370 equilibration due to micropores being blocked (Table 3) [15]. The reductions in Qm for the initial
 371 shales, SH1, SH2, BS3, and GH4 are 50, 66, 97, and 95%, respectively, which are larger than the
 372 extracted samples (40, 58, 96, and 81%, respectively), suggesting moisture has a slightly reduced
 373 impact for the extracted shales since they adsorbed less water (Table 1). Additionally, the methane
 374 adsorption capacities for the wet extracted shales are larger than for the initial shales (Table 3),

375 even considering the experimental errors (Figure 4). The Q_m of wet extracted SH1 increased from
376 39 to 59 mg/g TOC), SH2 from 44 to 55mg/g TOC, BS3 (from 0.4 to 1.3 mg/g TOC), and GH4 from 1.1
377 to 4.2 mg/g TOC), representing increases of 52, 27, 207 and 282% compared to the wet initial shales
378 (Table 3), consistent with the increase of accessible micropore volume for the extracted shales
379 (section 3.3).

380 For wet overmature shales, SH1 and SH2, the Henry's Law corrections for dissolved gas had virtually
381 no effect on the methane sorption capacities (Figure 4A and 4B). In contrast, the methane
382 adsorption isotherms after Henry's Law show negative isotherms for BS3 and GH4 (Figure 4C, and
383 4D). This indicates that virtually none of the methane is accessible to the oil. This arises from water
384 blocking the micropores or micropore necks. For both BS3 and GH4, solvent extraction significantly
385 increases the methane adsorption capacities, by a factor of 3-4, compared to the initial moisture
386 equilibrated shales by reducing the extent to which the pores are blocked by water.

387 4. GIP estimation

388 Understanding both the impact of extracted oil and moisture on porosity and gas adsorption
389 properties is vital for an accurate evaluation of shale gas resources and the design of effective
390 production strategies. Like moisture, the removal of oil generated by maturation can lead to an
391 overestimation of GIP [15]. Equation (3) has been used to calculate GIP in this study. The porosities
392 of the dry and wet shale used for calculating the free gas calculation are based on equations (4) and
393 (5). Considering the buried depths of the four samples, the reservoir pressure and temperature for
394 the overmature shales, SH1 and SH2, are estimated as 600 bar and 100 °C [15, 68] (Li et al., 2018;
395 Tang et al., 2016), for the UK Bowland shales, BS3, 300 bar and 60 °C and GH4, 450 bar and 80 °C.
396 The excess adsorbed gas content reduces about 45, 35, and 25 % at 100, 80, and 60 °C when
397 compared with 25 °C [12, 69, 70].

$$398 \quad GIP = Q_{free} + Q_a = Q_{free} + Q_e + V_a \times \rho_g = V_{tot} \times \rho_g + Q_e \quad (3)$$

$$399 \quad Porosity_{dry} = \frac{V_{dry\ pore}}{V_{sh}} = 1 - \frac{\rho_{dry\ bulk}}{\rho_{dry\ sk}} \quad (4)$$

$$400 \quad Porosity_{wet} = \frac{V_{wet\ pore}}{V_{sh}} = 1 - \frac{\rho_{wet\ bulk}}{\rho_{wet\ sk}} = 1 - \frac{\rho_{dry\ bulk}}{\rho_{wet\ sk}} \times (1 + W) \quad (5)$$

401 Where, Q_{free} is the free gas; Q_a is the absolute adsorption gas; Q_e is the excess adsorption gas; V_a
 402 is the pore volume for gas to adsorb into; ρ_g is the density of the bulk gas, which can be obtained
 403 from the REFPROP version 8.0 software; V_{tot} is the total pore volume accessible to gas in
 404 shale; $Porosity_{dry}$ is the total porosity of dry shale; $V_{dry\ pore}$ is the pore volume of dry
 405 shale; $Porosity_{wet}$ is the total porosity of wet shale; $V_{wet\ pore}$ is the pore volume of wet shale; V_{sh}
 406 is the shale sample volume; $\rho_{wet\ bulk}$ is the bulk density of wet shale, $\rho_{dry\ bulk}$ is the bulk density
 407 of dry shales from mercury intrusion porosimetry (MIP) at 0.035 bar, $\rho_{dry\ sk}$ and $\rho_{wet\ sk}$ are the
 408 skeletal densities of the dry and wet samples obtained from helium pycnometry; W is the moisture
 409 content.

410 The total porosity and GIPs estimated for the initial and extracted shales are compared in Table 4.

411 Oil extraction increased the total porosity from 18.3 to 21.0% for the dry shales, BS3, and increases
 412 from 16.8 to 20.9% for the moisture equilibrated shale, which are much larger increases than the
 413 other shales, as BS3 has the highest oil yield (Table 4). Table 4 indicates that the estimated GIP
 414 increases with total porosity, in the order of GH4>BS3>SH1>SH2 for the initial shales under both dry
 415 and moisture equilibrated conditions. Although SH1 and SH2 have much larger adsorbed gas (Q_a)
 416 contributions, the free gas (Q_{free}) contributions controlled by the total pore volume are smaller than
 417 for BS3 and GH4 (Table 3). However, in all cases, the free gas contributions dominate the GIP
 418 estimates for the initial dry shales (82, 65, 99, and 98% for SH1, SH2, BS3, and GH4, respectively,
 419 Table 4). As expected, the GIP estimated for the moisture equilibrated shales are lower than for dry
 420 shales, with reductions of 32, 38, 11, and 12% observed for initial SH1, SH2, BS3, and GH4,
 421 respectively, with the reductions for the extracted moisture equilibrated shales being 27, 28, 4 and
 422 14%, respectively, when compared with the corresponding extracted dry shales (Table 4). This
 423 confirms the GIP based on dry shales is significantly overestimated, as previous research indicated
 424 [15, 71, 72]. Moreover, moisture reduces the adsorbed gas (41-96%) more than the free gas (2-27%)

425 for both the initial and extracted shale (Table 4) since the impact of moisture is mainly blocking
 426 micropores for adsorbed gas rather than the larger pores accommodating most of the free gas.
 427 Table 4. The porosity, total pore volume, and the estimated GIP of the initial and extracted shales.

Sample Name	Porosity (%)	V_{total} (m ³ /t)	N_a (kg/t)	N_{free} (kg/t)	GIP (kg/t)	GIP change after extraction (%)
Dry Initial SH1	10.2	0.0432	2.1	9.3	11.4	6
Dry Ext SH1	10.2	0.0434	2.6	9.5	12.1	
Dry Initial SH2	4.0	0.0156	1.6	2.9	4.5	-3
Dry Ext SH2	3.8	0.0148	1.7	2.7	4.4	
Dry Initial BS3	18.3	0.0857	0.21	15.5	15.7	16
Dry Ext BS3	21.0	0.1008	0.44	18.2	18.7	
Dry Initial GH4	22.2	0.1046	0.44	22.8	23.2	3
Dry Ext GH4	22.8	0.1080	0.47	23.5	23.9	
Wet Initial SH1	6.8	0.0284	0.94	6.8	7.8	12
Wet Ext SH1	7.2	0.0304	1.5	7.3	8.8	
Wet Initial SH2	2.5	0.0095	0.49	2.3	2.8	11
Wet Ext SH2	2.7	0.0102	0.65	2.5	3.1	
Wet Initial BS3	16.8	0.0772	0.007	14.0	14.0	22
Wet Ext BS3	20.9	0.0990	0.022	17.9	18.0	
Wet Initial GH4	20.3	0.0930	0.023	20.3	20.3	1
Wet Ext GH4	20.2	0.0938	0.090	20.5	20.6	

428 V_{total} is the total pore volume calculated from the porosity of corresponding shales.
 429 Overall, the changes arising from oil extraction are relatively small for the two overmature shales,
 430 SH1, SH2, and the gas window shale, GH4 (-3 to 6% for the dry shales and 1-12% for the moisture
 431 equilibrated shales, Table 4) with the largest changes being for the oil window shale, BS3. In contrast,
 432 Table 4 indicates that the GIP is overestimated by 16 and 22% for both dry and moisture equilibrated
 433 extracted oil window shale, BS3.
 434 Clearly, the impact of solvent extraction on the estimated GIP is minimal for the two overmature
 435 shales investigated, especially compared to moisture (Table 4). In contrast, although some
 436 researchers believe removing oil in low maturity shale has little influence on methane adsorption
 437 [21], the impact of oil removal is significant for oil-window shales, with the GIP being over-estimated
 438 by 22% for the shale investigated here. For such shales, a combination of moisture equilibration and
 439 not extracting oil present generated by maturation is essential to obtain reliable GIP estimates.

440 5. Conclusions

441 1). Solvent extraction has limited impacts on the methane adsorption and pore texture for the dry
442 overmature shales, SH1 and SH2, with the small amounts of extractable oil arising from drilling mud
443 contamination. However, micropore volume and the methane adsorption capacities for the wet
444 over mature shales increased after solvent extraction, possibly due to the reductions in moisture
445 content, meaning there is reduced pore blocking.

446 2). More than 60% of the extractable oil resides in micro and mesopores for the oil-window BS3.
447 Removing the oil increased the nano micro, meso, and macropore volumes by up to nearly 300% for
448 the dry BS3 and GH4. The increases in methane adsorption capacities are proportionally greater for
449 the wet shales (207-282%) compared to the dry shales (90 and 3%).

450 3). Henry's Law estimations have indicated that the proportions of dissolved gas in the dry shale
451 samples is extremely small. For wet shales, not all the residual oil is accessible if water blocks some
452 of the micropores, which means the dissolved gas calculated by Henry's Law could be significantly
453 overestimated.

454 4). Solvent extraction increases the estimated GIP by 16% for the dry oil-window shale, BS3, and
455 moisture reduces the GIP of the initial BS3 shale by 11%. The GIP for extracted wet shale is
456 overestimated by 22%. The impact on GIP estimates was considerably less for the over-mature
457 shales due to their low extractable oil contents. Nevertheless, this study indicates the significant
458 impact that natural oil arising from maturation can have on the estimated GIP for oil-window shales.

459 Acknowledgments

460 The authors greatly acknowledge financial support from the National Environment Research Council
461 (Grant no: NE/C507002/1) and the Faculty of Engineering Research Excellence Ph.D. Scholarship for

462 Wei Li provided by the University of Nottingham. The British Geological Survey is acknowledged for
463 providing the cores for the UK shales.

464 **References**

- 465 [1] Barker F. Trondhjemite: definition, environment and hypotheses of origin.
466 Developments in petrology. Elsevier; 1979, p. 1-12.
- 467 [2] Eldridge RB. Oil contaminant removal from drill cuttings by supercritical extraction.
468 Industrial & engineering chemistry research 1996;35(6):1901-5.
- 469 [3] Qi Y, Ju Y, Cai J, Gao Y, Zhu H, Hunag C, et al. The effects of solvent extraction on
470 nanoporosity of marine-continental coal and mudstone. Fuel 2019;235:72-84.
- 471 [4] DiStefano VH, McFarlane J, Stack AG, Perfect E, Mildner DF, Bleuel M, et al. Solvent-
472 pore interactions in the Eagle Ford shale formation. Fuel 2019;238:298-311.
- 473 [5] Bernard S, Horsfield B. Thermal maturation of gas shale systems. Annual Review of
474 Earth and Planetary Sciences 2014;42:635-51.
- 475 [6] Dayal AM, Mani D. Shale gas: Exploration and environmental and economic impacts.
476 Elsevier; 2017.
- 477 [7] Tissot BP, Welte DH. Petroleum formation and occurrence. Springer Science & Business
478 Media; 2013.
- 479 [8] Curtis JB. Fractured shale-gas systems. AAPG bulletin 2002;86(11):1921-38.
- 480 [9] Gasparik M, Bertier P, Gensterblum Y, Ghanizadeh A, Krooss BM, Littke R. Geological
481 controls on the methane storage capacity in organic-rich shales. International Journal of
482 Coal Geology 2014;123:34-51.
- 483 [10] Ross DJ, Bustin RM. Shale gas potential of the lower Jurassic Gordondale member,
484 northeastern British Columbia, Canada. Bulletin of Canadian Petroleum Geology
485 2007;55(1):51-75.
- 486 [11] Ross DJ, Bustin RM. The importance of shale composition and pore structure upon gas
487 storage potential of shale gas reservoirs. Marine and petroleum Geology
488 2009;26(6):916-27.
- 489 [12] Rexer TF, Benham MJ, Aplin AC, Thomas KM. Methane adsorption on shale under
490 simulated geological temperature and pressure conditions. Energy & Fuels
491 2013;27(6):3099-109.
- 492 [13] Tang X, Ripepi N, Stadie NP, Yu L, Hall MR. A dual-site Langmuir equation for accurate
493 estimation of high pressure deep shale gas resources. Fuel 2016;185:10-7.
- 494 [14] Whitelaw P, Uguna CN, Stevens LA, Meredith W, Snape CE, Vane CH, et al. Shale gas
495 reserve evaluation by laboratory pyrolysis and gas holding capacity consistent with field
496 data. Nature communications 2019;10(1):1-10.
- 497 [15] Li W, Stevens LA, Uguna CN, Vane CH, Meredith W, Tang L, et al. Comparison of the
498 impact of moisture on methane adsorption and nanoporosity for over mature shales and
499 their kerogens. International Journal of Coal Geology 2021:103705.
- 500 [16] Rexer TF, Mathia EJ, Aplin AC, Thomas KM. High-pressure methane adsorption and
501 characterization of pores in Posidonia shales and isolated kerogens. Energy & Fuels
502 2014;28(5):2886-901.
- 503 [17] Guo S. Experimental study on isothermal adsorption of methane gas on three shale
504 samples from Upper Paleozoic strata of the Ordos Basin. Journal of Petroleum Science
505 and Engineering 2013;110:132-8.
- 506 [18] Wang Y, Zhu Y, Liu S, Zhang R. Pore characterization and its impact on methane
507 adsorption capacity for organic-rich marine shales. Fuel 2016;181:227-37.
- 508 [19] Löhr S, Baruch E, Hall P, Kennedy M. Is organic pore development in gas shales
509 influenced by the primary porosity and structure of thermally immature organic matter?
510 Organic Geochemistry 2015;87:119-32.
- 511 [20] Hu H, Zhang T, Wiggins-Camacho JD, Ellis GS, Lewan MD, Zhang X. Experimental
512 investigation of changes in methane adsorption of bitumen-free Woodford Shale with
513 thermal maturation induced by hydrous pyrolysis. Marine and Petroleum Geology
514 2015;59:114-28.

- 515 [21] Liu G, Huang Z, Jiang Z, Chen J, Chen F, Xing J. Gas adsorption capacity calculation
516 limitation due to methane adsorption in low thermal maturity shale: A case study from
517 the Yanchang Formation, Ordos Basin. *Journal of Natural Gas Science and Engineering*
518 2016;30:106-18.
- 519 [22] Ibad SM, Padmanabhan E. Methane sorption capacities and geochemical
520 characterization of Paleozoic shale Formations from Western Peninsula Malaysia:
521 Implication of shale gas potential. *International Journal of Coal Geology* 2020:103480.
- 522 [23] Cao Y, Han H, Liu H-w, Jia J-c, Zhang W, Liu P-w, et al. Influence of solvents on pore
523 structure and methane adsorption capacity of lacustrine shales: An example from a
524 Chang 7 shale sample in the Ordos Basin, China. *Journal of Petroleum Science and*
525 *Engineering* 2019;178:419-28.
- 526 [24] Mohnhoff D, Littke R, Krooss BM, Weniger P. Flow-through extraction of oil and gas
527 shales under controlled stress using organic solvents: Implications for organic matter-
528 related porosity and permeability changes with thermal maturity. *International Journal*
529 *of Coal Geology* 2016;157:84-99.
- 530 [25] Guo H, Jia W, Lei Y, Luo X, Cheng M, Wang X, et al. The composition and its impact on
531 the methane sorption of lacustrine shales from the Upper Triassic Yanchang Formation,
532 Ordos Basin, China. *Marine and Petroleum Geology* 2014;57:509-20.
- 533 [26] Berthezene N, De Hemptinne J-C, Audibert A, Argillier J-F. Methane solubility in
534 synthetic oil-based drilling muds. *Journal of Petroleum Science and Engineering*
535 1999;23(2):71-81.
- 536 [27] Jarrett AJ, Schinteie R, Hope JM, Brocks JJ. Micro-ablation, a new technique to remove
537 drilling fluids and other contaminants from fragmented and fissile rock material.
538 *Organic geochemistry* 2013;61:57-65.
- 539 [28] DiStefano VH, McFarlane J, Anovitz LM, Stack AG, Gordon AD, Littrell KC, et al.
540 Extraction of organic compounds from representative shales and the effect on porosity.
541 *Journal of Natural Gas Science and Engineering* 2016;35:646-60.
- 542 [29] Li W, Pang X, Snape C, Zhang B, Zheng D, Zhang X. Molecular Simulation Study on
543 Methane Adsorption Capacity and Mechanism in Clay Minerals: Effect of Clay Type,
544 Pressure, and Water Saturation in Shales. *Energy & Fuels* 2019;33(2):765-78.
- 545 [30] Tan J, Weniger P, Krooss B, Merkel A, Horsfield B, Zhang J, et al. Shale gas potential of
546 the major marine shale formations in the Upper Yangtze Platform, South China, Part II:
547 Methane sorption capacity. *Fuel* 2014;129:204-18.
- 548 [31] Simpson J, Dearing H. Diffusion Osmosis-An unrecognized cause of shale instability.
549 *IADC/SPE Drilling Conference*. Society of Petroleum Engineers; 2000.
- 550 [32] Loucks RG, Ruppel SC. Mississippian Barnett Shale: Lithofacies and depositional setting
551 of a deep-water shale-gas succession in the Fort Worth Basin, Texas. *AAPG bull*
552 2007;91(4):579-601.
- 553 [33] Heller R, Zoback M. Adsorption of methane and carbon dioxide on gas shale and pure
554 mineral samples. *Journal of Unconventional Oil and Gas Resources* 2014;8:14-24.
- 555 [34] Jin Z, Firoozabadi A. Effect of water on methane and carbon dioxide sorption in clay
556 minerals by Monte Carlo simulations. *Fluid Phase Equilibria* 2014;382:10-20.
- 557 [35] Ji L, Zhang T, Milliken KL, Qu J, Zhang X. Experimental investigation of main controls to
558 methane adsorption in clay-rich rocks. *Applied Geochemistry* 2012;27(12):2533-45.
- 559 [36] Zolfaghari A, Dehghanpour H, Xu M. Water sorption behaviour of gas shales: II. Pore
560 size distribution. *International Journal of Coal Geology* 2017;179:187-95.
- 561 [37] Merkel A, Fink R, Littke R. High pressure methane sorption characteristics of lacustrine
562 shales from the Midland Valley Basin, Scotland. *Fuel* 2016;182:361-72.
- 563 [38] Young JF. Humidity control in the laboratory using salt solutions—a review. *Journal of*
564 *Applied Chemistry* 1967;17(9):241-5.
- 565 [39] Zolfaghari A, Dehghanpour H, Holyk J. Water sorption behaviour of gas shales: I. Role
566 of clays. *International Journal of Coal Geology* 2017;179:130-8.
- 567 [40] Greenspan L. Humidity fixed points of binary saturated aqueous solutions. *Journal of*
568 *research of the national bureau of standards* 1977;81(1):89-96.
- 569 [41] Schoenherr J, Littke R, Urai JL, Kukla PA, Rawahi Z. Polyphase thermal evolution in the
570 Infra-Cambrian Ara Group (South Oman Salt Basin) as deduced by maturity of solid
571 reservoir bitumen. *Organic Geochemistry* 2007;38(8):1293-318.

- 572 [42] Brunauer S, Emmett PH, Teller E. Adsorption of gases in multimolecular layers. *Journal*
573 *of the American chemical society* 1938;60(2):309-19.
- 574 [43] Thommes M, Kaneko K, Neimark AV, Olivier JP, Rodriguez-Reinoso F, Rouquerol J, et al.
575 Physisorption of gases, with special reference to the evaluation of surface area and pore
576 size distribution (IUPAC Technical Report). *Pure and Applied Chemistry* 2015;87(9-
577 10):1051-69.
- 578 [44] Rouquerol J, Llewellyn P, Rouquerol F. Is the BET equation applicable to microporous
579 adsorbents. *Stud Surf Sci Catal* 2007;160(07):49-56.
- 580 [45] Qi L, Tang X, Wang Z, Peng X. Pore characterization of different types of coal from coal
581 and gas outburst disaster sites using low temperature nitrogen adsorption approach.
582 *International Journal of Mining Science and Technology* 2017;27(2):371-7.
- 583 [46] Bertier P, Schweinar K, Stanjek H, Ghanizadeh A, Clarkson CR, Busch A, et al. On the
584 use and abuse of N₂ physisorption for the characterization of the pore structure of
585 shales. *The clay minerals society workshop lectures series*. 21. 2016:151-61.
- 586 [47] Luo P, Zhong N, Khan I, Wang X, Wang H, Luo Q, et al. Effects of pore structure and
587 wettability on methane adsorption capacity of mud rock: Insights from mixture of
588 organic matter and clay minerals. *Fuel* 2019;251:551-61.
- 589 [48] Gregg S, Sing K. W. Adsorption, surface area and porosity. London: Academic Press
590 1982:195-7.
- 591 [49] Liu J, Sun N, Sun C, Liu H, Snape C, Li K, et al. Spherical potassium intercalated
592 activated carbon beads for pulverised fuel CO₂ post-combustion capture. *Carbon*
593 2015;94:243-55.
- 594 [50] Sircar S. Gibbsian surface excess for gas adsorption revisited. *Industrial & engineering*
595 *chemistry research* 1999;38(10):3670-82.
- 596 [51] Stasiuk L, Snowdon L. Fluorescence micro-spectrometry of synthetic and natural
597 hydrocarbon fluid inclusions: crude oil chemistry, density and application to petroleum
598 migration. *Applied Geochemistry* 1997;12(3):229-41.
- 599 [52] Hanafy H, Macary S, ElNady Y, Bayomi A, El Batanony M. A new approach for predicting
600 the crude oil properties. *SPE Production Operations Symposium*. Society of Petroleum
601 Engineers; 1997.
- 602 [53] Andrews IJ. The Carboniferous Bowland Shale gas study: geology and resource
603 estimation. 2013.
- 604 [54] Clarke H, Turner P, Bustin RM, Riley N, Besly B. Shale gas resources of the Bowland
605 Basin, NW England: a holistic study. *Petroleum Geoscience* 2018;24(3):287-322.
- 606 [55] Wenger LM, Davis CL, Evensen JM, Gormly JR, Mankiewicz PJ. Impact of modern
607 deepwater drilling and testing fluids on geochemical evaluations. *Organic geochemistry*
608 2004;35(11-12):1527-36.
- 609 [56] Curtis ME, Cardott BJ, Sondergeld CH, Rai CS. Development of organic porosity in the
610 Woodford Shale with increasing thermal maturity. *International Journal of Coal Geology*
611 2012;103:26-31.
- 612 [57] Gasparik M, Ghanizadeh A, Bertier P, Gensterblum Y, Bouw S, Krooss BM. High-
613 pressure methane sorption isotherms of black shales from the Netherlands. *Energy &*
614 *fuels* 2012;26(8):4995-5004.
- 615 [58] Hu H. Methane adsorption comparison of different thermal maturity kerogens in shale
616 gas system. *Chinese Journal of Geochemistry* 2014;33(4):425-30.
- 617 [59] Mastalerz M, Hampton L, Drobnik A, Loope H. Significance of analytical particle size in
618 low-pressure N₂ and CO₂ adsorption of coal and shale. *International Journal of Coal*
619 *Geology* 2017;178:122-31.
- 620 [60] Cao T, Song Z, Wang S, Xia J. A comparative study of the specific surface area and
621 pore structure of different shales and their kerogens. *Science China Earth Sciences*
622 2015;58(4):510-22.
- 623 [61] Tissot B. Recent advances in petroleum geochemistry applied to hydrocarbon
624 exploration. *AAPG Bulletin* 1984;68(5):545-63.
- 625 [62] Katsube T. Shale permeability and pore-structure evolution characteristics. *Natural*
626 *Resources Canada, Geological Survey of Canada*; 2000.
- 627 [63] Best M, Katsube T. Shale permeability and its significance in hydrocarbon exploration.
628 *The Leading Edge* 1995;14(3):165-70.

- 629 [64] Alfi M, Barrufet M, Killough J. Effect of pore sizes on composition distribution and
630 enhance recovery from liquid shale—Molecular sieving in low permeability reservoirs.
631 Fuel 2019;235:1555-64.
- 632 [65] Lee S, Fischer TB, Stokes MR, Klingler RJ, Ilavsky J, McCarty DK, et al. Dehydration
633 effect on the pore size, porosity, and fractal parameters of shale rocks: Ultrasmall-angle
634 X-ray scattering study. Energy & fuels 2014;28(11):6772-9.
- 635 [66] Chen J, Xiao X. Evolution of nanoporosity in organic-rich shales during thermal
636 maturation. Fuel 2014;129:173-81.
- 637 [67] Job N, Théry A, Pirard R, Marien J, Kocon L, Rouzaud J-N, et al. Carbon aerogels,
638 cryogels and xerogels: Influence of the drying method on the textural properties of
639 porous carbon materials. Carbon 2005;43(12):2481-94.
- 640 [68] Li J, Zhou S, Gaus G, Li Y, Ma Y, Chen K, et al. Characterization of methane adsorption
641 on shale and isolated kerogen from the Sichuan Basin under pressure up to 60 MPa:
642 Experimental results and geological implications. International Journal of Coal Geology
643 2018;189:83-93.
- 644 [69] Zou J, Rezaee R, Liu K. Effect of temperature on methane adsorption in shale gas
645 reservoirs. Energy & Fuels 2017;31(11):12081-92.
- 646 [70] Ji W, Song Y, Jiang Z, Chen L, Li Z, Yang X, et al. Estimation of marine shale methane
647 adsorption capacity based on experimental investigations of Lower Silurian Longmaxi
648 formation in the Upper Yangtze Platform, south China. Marine and Petroleum Geology
649 2015;68:94-106.
- 650 [71] Chalmers GR, Bustin MR. PS The Effects and Distribution of Moisture in Gas Shale
651 Reservoir Systems. AAPG Annual Convention and Exhibition 2010.
- 652 [72] Krooss Bv, Van Bergen F, Gensterblum Y, Siemons N, Pagnier H, David P. High-
653 pressure methane and carbon dioxide adsorption on dry and moisture-equilibrated
654 Pennsylvanian coals. International Journal of Coal Geology 2002;51(2):69-92.

655